ACS APPLIED MATERIALS & INTERFACES

Research Article

www.acsami.org

Robust Superhydrophobic Bridged Silsesquioxane Aerogels with Tunable Performances and Their Applications

Zhen Wang,[†,‡] Dong Wang,[†,‡] Zhenchao Qian,[†,‡] Jing Guo,[†,‡] Haixia Dong,[†] Ning Zhao,*[,†] and Jian Xu*[,†]

[†]Beijing National Laboratory for Molecular Sciences, Laboratory of Polymer Physics and Chemistry, Institute of Chemistry, Chinese Academy of Sciences, Beijing 100190, China

[‡]University of Chinese Academy of Sciences, Beijing 100049, China

Supporting Information

ABSTRACT: Aerogels are a family of highly porous materials whose applications are commonly restricted by poor mechanical properties. Herein, thiol-ene chemistry is employed to synthesize a series of novel bridged silsesquioxane (BSQ) precursors with various alkoxy groups. On the basis of the different hydrolyzing rates of the methoxy and ethoxy groups, robust superhydrophobic BSQ aerogels with tailorable morphology and mechanical performances have been prepared. The flexible thioether bridge contributes to the robustness of the as-formed aerogels, and the property can be tuned on the basis of the distinct combinations of alkoxy groups with the density of the aerogels almost unchanged. To the best of our knowledge, the lowest density among the ambient pressure dried aerogels is obtained. Further, potential application of the aerogels for oil/water separation and acoustic materials has also been presented.

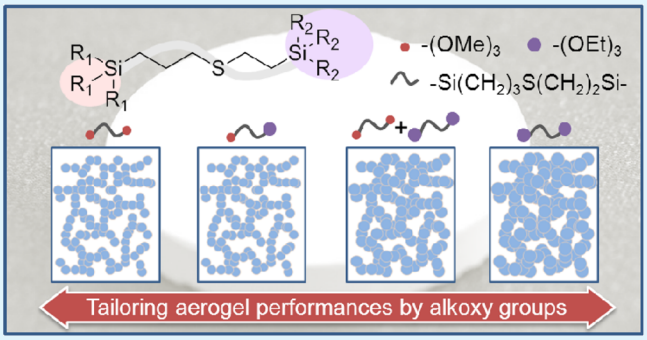

KEYWORDS: *aerogel, alkoxy group, bridged silsesquioxane, robustness, oil/water separation*

1. INTRODUCTION

Aerogels, first created by Kistler in 1931, are highly porous materials derived from gels, of which the liquid component is replaced by air and the porous structure is mostly maintained.[1] Known for low density, large porosity, high specific surface area (SSA), and low thermal conductivity,[2−5] aerogels have drawn interests in various applications, including sensors,[6] optical devices,[7] heat insulators,[8] absorbents,[9,10] catalysis,[11,12] and some aerospace applications.[13,14] Recently, with the rapid development of carbonaceous aerogels,[15−20] the applications are extended to electrochemical devices,[21−23] oil/water separations,[24,25] and so on. However, practical applications of aerogels, especially the most developed silica aerogels, have always been restricted due to their fragility.[14,26] By far, efforts aiming to toughen silica aerogels generally induce an increased density which deviates from low density, the most significant characteristic of aerogels.[27,28] Besides, approaches for tailoring the properties are confined to changing the monomer concentrations,[28,29] catalyst species,[30] and additives[31] in sol−gel processes. These methods do adjust the properties of the aerogels, such as mechanical properties or morphology, but at the expense of other parameters like an increased density. To the best of our knowledge, there are few reports about tuning the performance of aerogels without changing the composition or sacrificing the density.

Bridged silsesquioxane (BSQ) aerogels, a family of inorganic−organic molecularly hybrid materials generally derived from bridged silane precursors, exhibit distinct properties from traditional inorganic silica aerogels.[32−34] The variable organic bridges and the two or more hydrolyzable trifunctional silyl groups of the precursors offer the BSQ materials considerable flexibility to tune the performances inherently.[35−37] For example, because of the stiff bridge, the phenylene-bridged silsesquioxane aerogel obtained a 5-fold greater strength than the silica aerogel with the same density.[38] Soft and durable aerogels have been prepared from precursors containing flexible thioether or dipropyl sulfide bridging groups.[39,40] Surface areas of alkylene-bridged silsesquioxane aerogels decreased with the increase of the chain length of alkylene bridges.[41] However, the influence of the trifunctional silyl groups on the performances of BSQ aerogels seems to be neglected.[42] It has been demonstrated that the different hydrolyzing rates of the alkoxysilanes resulted in the formation of silica particles with various diameters and morphologies.[43,44] Thus, it might be possible to tune the properties of BSQ aerogels by changing the alkoxy groups of the precursors.

Received: November 9, 2014
Accepted: January 5, 2015
Published: January 5, 2015

DOI: 10.1021/am5077765
ACS Appl. Mater. Interfaces 2015, 7, 2016−2024

Scheme 1. (a) Synthesis of the Precursors, R_1, R_2 = OMe or OEt; (b) Procedure of Preparing Aerogels

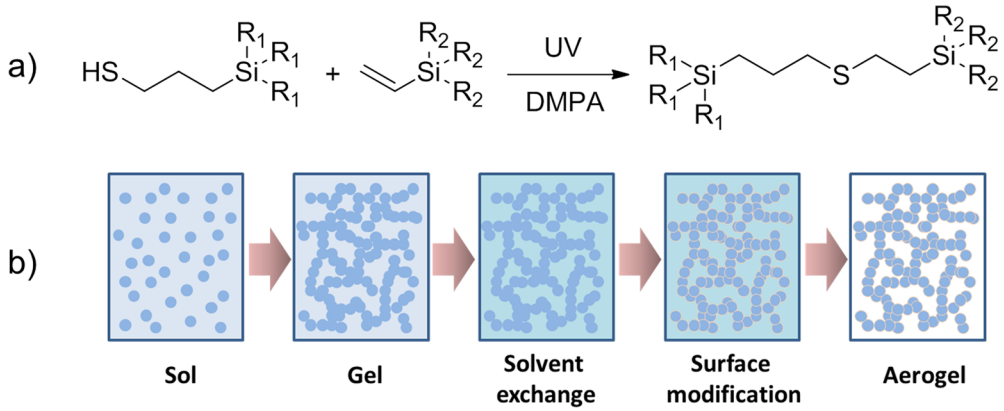

Previously, we first synthesized a new thioether BSQ precursor by a thiol-ene reaction and prepared flexible BSQ aerogels by a vacuum-drying method.[39] In this study, a series of thioether BSQ precursors with different alkoxy groups are synthesized (Scheme 1a). BSQ aerogels are obtained by ambient pressure drying (APD) (Scheme 1b). It has been found that the alkoxy groups of the precursors have profound influences on the aerogel performance. The low density, excellent flexibility, and tunable morphology and mechanical property make the BSQ aerogels prepared distinct from the APD aerogels reported before. Potential application of the resultant BSQ aerogels in oil/water separation and sound absorption has been presented.

2. EXPERIMENTAL SECTION

Materials. Vinyltrimethoxysilane (VTMS, 98%), 3-mercaptopropyltrimethoxysilane (MPTMS, 95%), and 3-mercaptopropyltriethoxysilane (MPTES, 94%) were purchased from Alfa Aesar. Triethoxyvinylsilane (TEVS, 97%) was a product of Sigma-Aldrich. 2,2-Dimethoxy-2-phenyl acetophenone (DMPA, 99%) was gotten from Acros. Trimethylchlorosilane (TMCS, 98%) was a product of Sinopharm Chemical Reagent Co., Ltd., China. Hydrochloric acid (37 wt % aqueous solution), ethanol, *n*-hexane, and toluene of analytical grade were obtained from Beijing Chemical Reagents Co., China. All the reagents were used without further purification.

Synthesis of BSQ Precursors. The precursors are designated as P1, P2, P3, and P4. P1 represents 2-(trimethoxysilyl)ethyl-3-(trimethoxysilyl)propylsulfide whose R_1 and R_2 are both methoxy groups. P2 represents 2-(triethoxysilyl)ethyl-3-(trimethoxysilyl)-propylsulfide whose R_1 is a methoxy group and R_2 is an ethoxy group. P4 represents 2-(triethoxysilyl)propyl-3-(triethoxysilyl)-ethylsulfide whose R_1 and R_2 are both ethoxy groups. P1, P2, and P4 were synthesized by the thiol-ene reactions. P3 is the mixture of P1 and P4 with equal mole. Here, we take P1 as an example to describe the synthesis processes. MPTMS (9.29 mL, 0.05 mol) and VTMS (7.66 mL, 0.05 mol) were put into a 25 mL round-bottom flask, and then DMPA (0.1282 g, 0.5 mmol) was added to initiate the reaction. The mixture was irradiated by a 365 nm mercury lamp for 4 h at room temperature under stirring. All the products were used directly to prepare aerogels without further purification.

Preparation of Aerogels. Hydrochloric acid and precursor with a fixed molar ratio of H^+/Si at 3.5 in all experiments were added into ethanol and stirred for 10 min. The resultant sol was poured into molds and put in an oven at 60 °C for gelation. After sufficient aging, the obtained gels were transferred from the molds into an ethanol bath. The gels were soaked in ethanol for 72 h during which the liquid was exchanged by fresh ethanol three times a day to completely remove the residual water and byproducts. Then, the gels were dried by ambient pressure drying according to a previously reported method.[45] The alcogels were submersed in *n*-hexane, and the solvent was exchanged six times. After that, *n*-hexane was replaced by sufficient TMCS/*n*-hexane solution (1/9 in volume) and the gels were put in an oven at 55 °C for 24 h. The modified gels were then washed twice by fresh *n*-hexane. The BSQ aerogels were obtained after being dried in the oven at 60 °C for 12 h, 80 °C for 2 h, and 120 °C for 2 h.

Characterization. ^{1}H NMR and ^{13}C NMR study was carried out on a Bruker 400 M instrument using deuterated chloroform as solvent. ^{29}Si solid NMR investigation was performed on Avance III 400, a Bruker production. For the ^{29}Si solid state NMR investigation, the gels were vacuum-dried before reacting with TMCS in order to avoid the further increased degree of condensation (DC) caused by the reaction between Si−OH and TMCS. The DC is calculated from the peak areas of T^2 (−59 ppm) and T^3 (−67 ppm) according to the following equation: $DC = (T^1 + 2T^2 + 3T^3)/3$, where T^i refers to the R−Si(OSi)$_i$(OR′)$_{3-i}$ species (R′ = H, Me, or Et). Fourier transform infrared spectroscopy (FT-IR) was performed on a Bruker TENSOR-27 by coating the liquid samples on KBr slices. Mass spectra were acquired on a Bruker Autoflex III time-of-flight mass spectrometer. The mechanical properties were studied on a WDT-10 tensile tester (Shenzhen Kaiqiangli Testing Instrument Co., Ltd). The columniform specimens were loaded in a compression mode with a rate of 0.5 mm/min. Scanning electron microcopy (SEM) was performed on a JEOL JSM-7500F at an accelerating voltage of 5 kV. Water contact angles were characterized using a KRÜSS DSA 100 by a sessile drop method. The droplets were all 10 μL in volume. Nitrogen-adsorption porosimetry was performed at 77 K on a TriStar II 3020 specific surface area and porosity analyzer, a production of Micromeritics Instrument Corporation. The samples were outgassed at 150 °C for 8 h before the tests. Thermal conductivity was measured on a Hot Disk 2500s thermal constants analyzer, which was based on transient plane sources. The skeletal density was measured by an UltraPYC 1200e automatic density analyzer, an instrument from Quantachrome. The porosities were calculated by the equation, porosity = $(1 - \rho_b/\rho_s) \times 100\%$, where ρ_b and ρ_s are densities of the bulk and the skeleton of the aerogels, respectively. Normal incidence sound absorption was measured on aerogels of 9 mm in thickness by type SW 466 Impedance Tubes, a production of BSWA Technology Co., Ltd. (China), based on ISO10534-2:1998(E) (Acoustics−Determination of sound absorption coefficient and impedance in impedance tubes-Part 2: Transfer function method). The acoustic tests were carried out at 27 °C and 60% relative humidity.

3. RESULTS AND DISCUSSION

3.1. Precursor Synthesis. The precursors were synthesized by the thiol-ene reaction of 3-mercaptopropyl and vinyl trialkoxysilanes, as shown in Scheme 1a. Thiol-ene reactions, which have been widely used to create new compounds,[46−50] are effective to synthesize the bridged precursors with demanded alkoxy groups. The stoichiometric reactions have high yields under mild conditions and are amenable to a variety

DOI: 10.1021/am5077765
ACS Appl. Mater. Interfaces 2015, 7, 2016−2024

of available compounds.[51] Therefore, the bridged precursors with the specific alkoxy groups could be facilely synthesized in high yields and purities from commercially available silanes. According to the ^{1}H NMR and FT-IR results (Figure 1 and

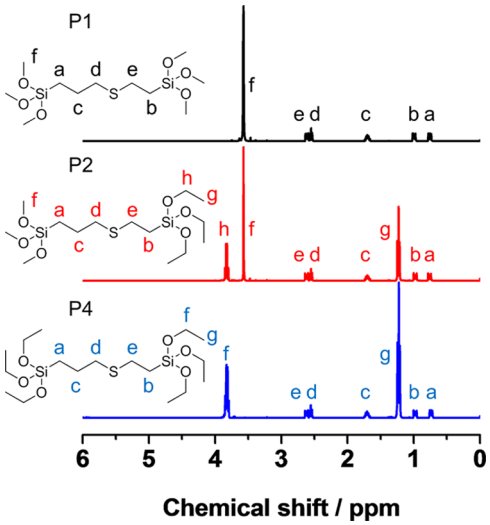

Figure 1. ^{1}H NMR spectra of the synthesized BSQ precursors.

Figures S1−S6, Supporting Information), the —SH and C═C double bonds of the reactants are mostly consumed and the reactions present high conversions of 96, 97, and 96%, as calculated from the peak area ratios of b/a in ^{1}H NMR spectra, for P1, P2, and P4, respectively. The high conversions ensured accurate synthesis of the precursors (Figures S7−S12, Supporting Information, ^{13}C NMR and TOF mass spectra) in high purities, which permit direct use in the following sol−gel processes without further purifications.

3.2. Sol−Gel Process. In general, the xerogels (or vacuum-dried aerogels[39]) possess high DCs ranging from 77.1 to 90.3%, as listed in Figure 2, which confirm the gelation is fully carried out and the mechanical stability of the later APD aerogels is guaranteed as a result. It has been reported that the alkoxy groups have distinct hydrolyzing rates.[43] The methoxy group hydrolyzes faster than the ethoxy group. From the ^{29}Si solid state NMR spectra, it can be clearly seen that the T^3 possesses a larger portion than T^2 as the amount of ethoxy groups increases in the precursors. That means the BSQ gels derived from P1, which hydrolyzes faster, have the lowest DC. The reason can be ascribed to the variation of the hydrolyzing rates of the different alkoxy groups. In the sol−gel process, abundant Si−OH groups are formed from the fast hydrolyzed methoxy groups in a short period of time. Part of the Si−OH groups condense and form the network through Si−O−Si bonds, which confine the location and increase the steric hindrance of the adjacent Si−OH. Therefore, many Si−OH groups are left uncondensed. In contrast, the ethoxy groups hydrolyze slowly. The slow rate gives the existing Si−OH groups enough time to be fully condensed with each other, leading to a high DC as a result. Therefore, the methoxy groups lead to a lower DC while the ethoxy groups result in a higher DC. The difference in hydrolyzing rates is also reflected in the texture differences, as shown in Figure 3. It is worth noting that, even though the xerogels discussed in this section are not the final APD aerogels in Figure 3, the textures of the xerogels and the APD aerogels are almost the same, as demonstrated in our previous work.[39]

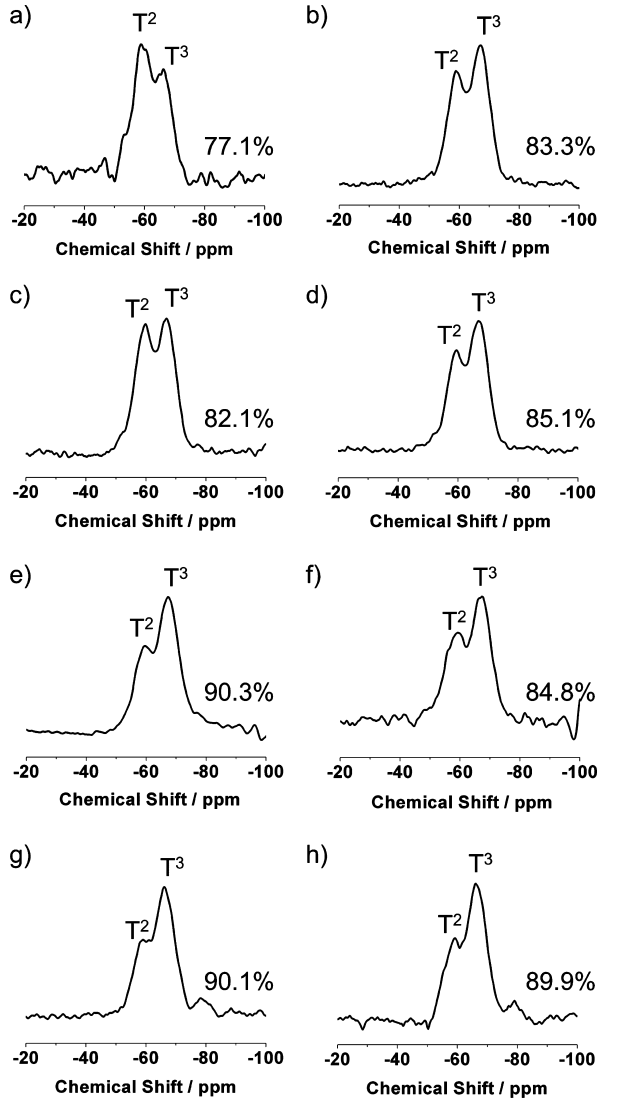

Figure 2. ^{29}Si solid state NMR spectra and DCs of the samples derived from (a) P1, 0.30 mol L^{-1}; (b) P1, 0.40 mol L^{-1}; (c) P2, 0.30 mol L^{-1}; (d) P2, 0.40 mol L^{-1}; (e) P3, 0.30 mol L^{-1}; (f) P3, 0.40 mol L^{-1}; (g) P4, 0.30 mol L^{-1}; and (h) P4, 0.40 mol L^{-1}.

Xerogels derived from P1 have smaller particle diameters and larger specific surfaces containing uncondensed bare Si−OH, while, in the xerogels derived from P4, the particle diameters are larger and bare surfaces are much less. The phenomena are in agreement with the silica particles derived from precursors containing different alkoxy groups: the diameter of the silica particles increases in the order of the hydrolyzing rates of methoxy, ethoxy, propoxy, and butoxy.[43]

3.3. Aerogel Characterization. The gels are dried by APD to form aerogels, which are designated as A1−A4 corresponding to the precursors from P1 to P4. The aerogels prepared exhibit good integrities and low apparent densities, compared to previously reported APD aerogels which are prone to be broken down to fragments[3,52] or with increased densities.[53] The properties of the aerogels are listed in Table 1. It is noteworthy that gelation was difficult to carry out when the precursor concentration was less than 0.30 mol L^{-1} for P2, P3, and P4.

Morphology. Figure 3 shows the morphology of the aerogels. In common, the aerogels are constructed by the

DOI: 10.1021/am5077765
ACS Appl. Mater. Interfaces 2015, 7, 2016−2024

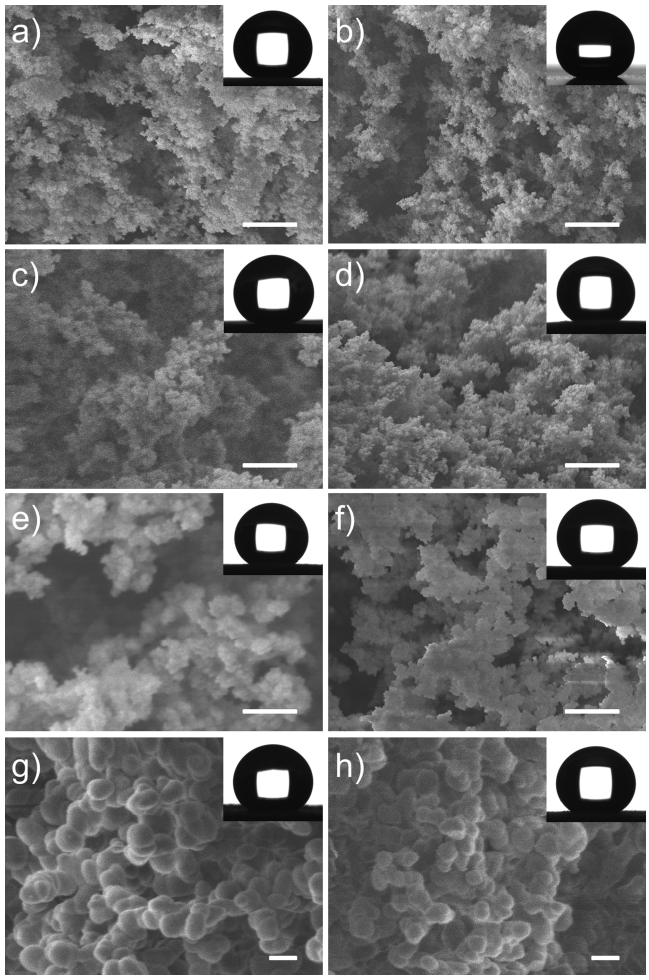

Figure 3. SEM micrographs of aerogels (a) A1, 0.30 mol L^{-1}; (b) A1, 0.40 mol L^{-1}; (c) A2, 0.30 mol L^{-1}; (d) A2, 0.40 mol L^{-1}; (e) A3, 0.30 mol L^{-1}; (f) A3, 0.40 mol L^{-1}; (g) A4, 0.30 mol L^{-1}; and (h) A4, 0.40 mol L^{-1}. The scale bars are 2 μm. The insets are photographs of water droplets on the surfaces of the samples.

randomly aggregated particles. The particles become smaller and the networks turn finer as the monomer concentration increases. The change tendency is in agreement with previous reports.[54,55] The reason is probably that monomers of a high concentration give a shorter gelation time, which restrains the particle to grow in sizes. In contrast, the particles have enough time to grow larger due to the long gelation time for the monomers of a low concentration.

The differences show up when the precursors are changed. A1 and A2 have highly porous networks loosely packaged by nanoparticles of approximate 100 nm in diameters. A4 shows a distinct morphology with the frameworks stacked by microparticles of about 1−2 μm in diameter. The texture of A3 falls somewhere in between those of A1 and A4, built up by particles of 200−500 nm in diameter. Obviously, alkoxy groups affect the morphology of the aerogel deeply. This is because methoxy groups hydrolyze faster than ethoxy groups in the acid catalyzed sol−gel process of BSQ precursors.[56] The difference makes nucleation more preferable for the precursors containing methoxy groups, while particle growth is favored for the precursors with ethoxy groups.[43] The preferences consequently induce the texture differences between A1 and A4 that A1 are constructed by much smaller particles than A4 are. Interest-

Table 1. Physical Properties of the BSQ Aerogels

category	precursor	the combination of alkoxy groups	precursor concentration (mol L^{-1})	density (g cm^{-3})	porosity (%)	SSA[a] (m^2 g^{-1})	pore size[b] (nm)	pore volume[c] (cm^3 g^{-1})	total pore volume[d] (cm^3 g^{-1})	Young's modulus (KPa)	thermal conductivity (mW m^{-1} K^{-1})	water contact angle (deg)
A1	P1	$(MeO)_3Si-R-Si(OMe)_3$	0.25	0.055	96.6	325	4.4	0.22	0.26	9.7	35.7	160
			0.30	0.063	96.3	368	7.5	0.57	0.58	29.3	33.8	170
			0.35	0.074	95.6	324	7.4	0.43	0.46	50.6	35.9	161
			0.40	0.079	95.3	373	8.3	0.64	0.66	139.2	35.6	162
A2	P2	$(MeO)_3Si-R-Si(OEt)_3$	0.30	0.062	96.3	307	5.9	0.30	0.34	19.7	36.0	169
			0.40	0.083	95.0	338	7.5	0.48	0.50	92.0	36.0	162
A3	P3 (mixture of P1 and P4)	$(MeO)_3Si-R-Si(OMe)_3$ and $(EtO)_3Si-R-Si(OEt)_3$	0.30	0.062	96.3	283	3.4	0.20	0.32	7.8	43.0	156
			0.40	0.075	95.4	283	3.4	0.20	0.31	58.0	42.3	160
A4	P4	$(EtO)_3Si-R-Si(OEt)_3$	0.30	0.065	96.0	65	4.9	0.02	0.04	7.2	36.3	155
			0.40	0.075	95.4	90	4.7	0.03	0.05	18.8	37.5	155

[a]Brunauer−Emmet−Teller (BET) surface area. [b]Barrett−Joyner−Halenda (BJH) adsorption average pore diameter. [c]BJH adsorption cumulative volume of pores between 17 and 3000 Å diameter. [d]Calculated according to the quantity adsorbed at P/P_0 = 0.995.

DOI: 10.1021/am5077765
ACS Appl. Mater. Interfaces 2015, 7, 2016−2024

ingly, the morphology of A2 and A3 shows an evident discrepancy even though the corresponding precursors have the same molar ratio of methoxy and ethoxy groups. Instead, A2 has a similar morphology to that of A1, but A3 is less similar to A1. The result is contradictory to common sense that the morphology should correspond to the proportion of alkoxy groups of the precursors. In other words, A2 and A3 are supposed to show a similar morphology which is different from A1. The experiment results indicate that the morphology is determined not only by the composition of alkoxy groups but also by the connection manner between different alkoxy groups. For P2 containing both methoxy and ethoxy groups in the molecule, it is the hydrolysis and condensation of the methoxy groups that mainly contribute to the formation of gel networks. The ethoxy has a lesser contribution to the formation of the network; therefore, the resultant aerogel A2 has a similar morphology to A1. On the other hand, for the mixture of P1 and P4, assigned as P3, whose methoxy and ethoxy groups are not connected in the same molecule, the more reactive P1 leads to the formation of a primary skeleton and the less reactive P4 tends to hydrolyze and condense on the surface of the already formed P1 backbone; thus, A3 has a middling texture between A1 and A4.

In order to quantify the morphology difference, nitrogen sorption analysis was employed to examine surface areas, pore volumes, and pore sizes of the aerogels. The isotherms of BSQ aerogels, as shown in Figure 4, combine characters of type II

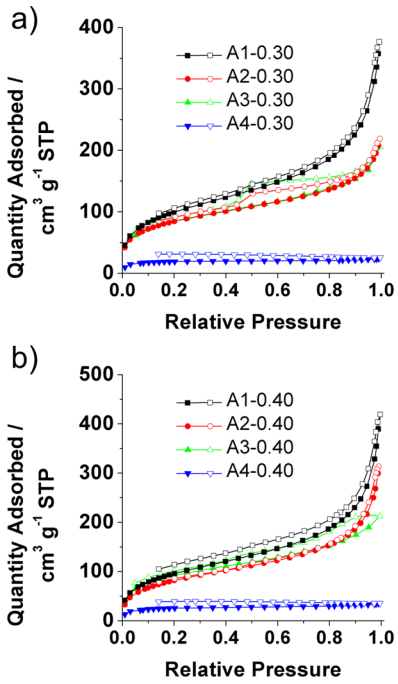

Figure 4. Nitrogen adsorption−desorption isotherms of the BSQ aerogels prepared with a monomer concentration of (a) 0.30 mol L^{-1} and (b) 0.40 mol L^{-1}.

and IV in IUPAC classification, indicating that both macro- and mesopores exist.[57,58] The BJH pore volumes are comparable with total pore volumes (Table 1), and the quantity absorbed at a relative pressure below 0.01 is low. The results suggest that no micropores exist. Since the mesopores of the aerogels are built by the stack of the primary particles with diameters of at least 100 nm, the pore sizes are not uniform and show no obvious peaks but a gradual decrease with increasing pore diameter (Figure S13, Supporting Information). A1 has the largest SSA (324−373 m^2 g^{-1}) and the largest pore volume (as large as 0.64 cm^3 g^{-1}) as compared with the other counterparts. In contrast, A4 has the lowest SSA (65 and 90 m^2 g^{-1}) and pore volume (0.02 and 0.03 cm^3 g^{-1}). The data is in agreement with the SEM observations shown in Figure 3, quantitatively confirming that A1 has finer structures than A2 than A3 than A4 does.

Density, Porosity, and Thermal Conductivity. As listed in Table 1, the density increases while the porosity decreases with the increase of monomer concentration. The densities and porosities of the aerogels derived from different precursors at the same concentration do not show obvious distinctions. The densities range from 0.055 to 0.083 g cm^{-3}, while the porosities are higher than 95.0% for the aerogels prepared. To the best of our knowledge, 0.055 g cm^{-3} is the lowest density ever acquired for aerogels produced by APD. The flexible thioether segments are believed to contribute to maintaining the low densities of the aerogels. During the APD process, the soft frameworks of the gels are able to change the configuration to bear the capillary force created by the liquid evaporation, withstand the destruction of shrinking, and finally spring back to their initial sizes. Moreover, the relative low polarity of the thioether bridge, compared to those containing hydroxyl, amino, or other polar groups, also helps reduce the interaction between the solvent and the gel skeleton, consequently minimizing the capillary force. Therefore, all the precursors build up highly cross-linked and firm enough gel networks to maintain the gel sizes in the drying process, and low apparent densities are obtained as a result.

Since the densities of the BSQ aerogels are low and the porosities are quite high, the thermal conductivities of the aerogels ranging from 33.8 to 43.0 mW m^{-1} K^{-1} are not as low as expected. It is known that thermal conductivities of aerogels are contributed by three parts: solid conductivity, gaseous conductivity, and radiative conductivity. Radiative conductivity is fixed when there is no opacifier integrated into aerogels; solid conductivity goes up with the increased aerogel density because the higher solid content brings more effective solid thermal conduction; gaseous conductivity goes down with the increased density because a higher solid content would result in a smaller pore size which suppresses gaseous thermal conductivity.[59] Therefore, it is reasonable that the BSQ aerogels presented in this work (opaque in appearance) have higher thermal conductivities than typical silica aerogels (17−21 mW m^{-1} K^{-1})[2] because the pore sizes are not small enough to confine gaseous thermal conductivity.

Mechanical Properties. The BSQ aerogels are flexible which can withstand at least 50% deformation under compressions without any detectable structural fracture, demonstrating excellent mechanical performances (Figure 5). The flexibility roots not only in the large porous feature of the BSQ aerogels which provides sufficient free space for squeezing the network but also in the nature of thioether segment in the BSQ molecular structure. The six-membered organic chain is quite flexible considering that the internal rotation barrier of carbon−sulfur bond (8.8 kJ mol^{-1}) is even lower than that of the carbon−carbon single bond in the alkyl chain (13.8 kJ mol^{-1}). The low barrier means an easier configuration change in the microscope when strain is loaded.

The Young's moduli of the BSQ aerogels prepared increase with the precursor concentration (Table 1). Moreover, the mechanical performances can be adjusted by the alkoxy groups

DOI: 10.1021/am5077765
ACS Appl. Mater. Interfaces 2015, 7, 2016−2024

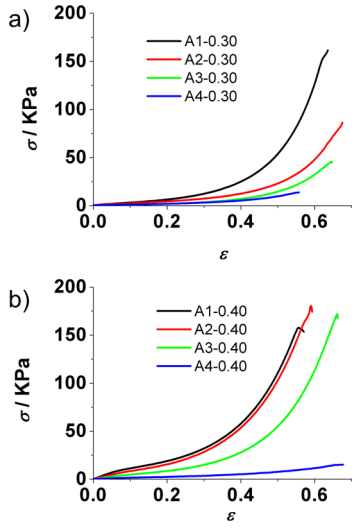

Figure 5. Stress–strain curves of the BSQ aerogels with a precursor concentration of (a) 0.3 mol L^{-1} and (b) 0.4 mol L^{-1}.

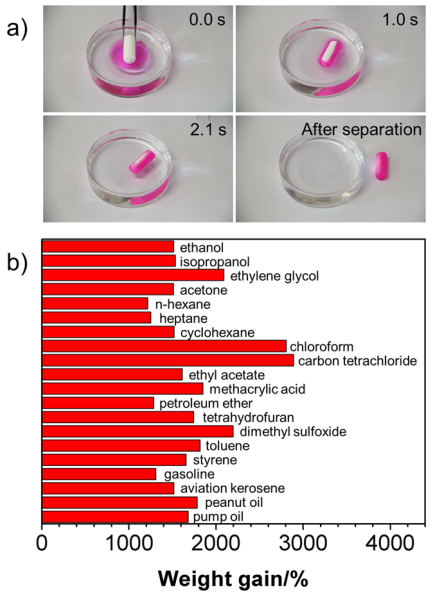

Figure 6. (a) Photos showing the separation of toluene (dyed with dil-C18) from water. (b) Absorption capacity of the BSQ aerogels for various organic liquids.

of the precursors because of the distinct microstructures resulting from the different alkoxy groups. The compression moduli of the BSQ aerogels at the same monomer concentration decrease in the order of A1 > A2 > A3 > A4, which is in good agreement with the change tendency of morphology fineness (Figure 5). Therefore, the mechanical performances of BSQ aerogels can be tailored precisely by designing the proportion and the connection manner of the alkoxy groups in the precursors. Besides, the compressive moduli of the BSQ aerogels varied with density as $\sim\rho^{6.3}$. The power of 6.3 is higher than the power of 1 of the 3D ordered nanofiber aerogel[29] and the common value of silica aerogels (between 2.0 and 3.6),[60,61] which means the density strongly decides the modulus and the strain transfer through the networks is inefficient. This is rooted from the acid-catalyzed sol–gel process which created more heterogeneous network structures with more dangling, nonbridging skeletons compared with the common two-step acid–base catalyzing.

3.4. Application in Oil/Water Separation. Since the surface of the nanostructured skeleton of BSQ aerogels has been modified by TMCS, a low surface energy was obtained after the modification. Because of the combination of the rough microstructure and the low surface energy, the resultant APD aerogels are superhydrophobic. Water contact angles (WCAs) on the aerogels are larger than 150° (Table 1 and insets in Figure 3), and the water droplets slid off the surface easily. It is known that the superhydrophobicity results from the rough nanostructure and the low surface energy of the aerogels.[62,63] The superhydrophobicity of aerogels is of advantage in long-term stability for practical applications. The superhydrophobic surface is hard to adsorb water, thus avoiding the crack induced by the capillary forces created by the condensation of moisture inside the bulk of the aerogels.[64,65] Besides, preventing water absorption also helps to keep the low density and high porosity and maintain the low thermal conductivity, which are critical for the application of aerogels.

The robust superhydrophobic aerogel monoliths are also suitable for the application in oil/water separation. The penetrated meso- and macropores provide abundant capillaries which help to realize a fast absorption of oil from the oil/water mixture. As revealed in Figure 6a, 1.073 g of toluene dyed by dil-C18 is completely absorbed within 2.1 s by a 91 mg aerogel. The toluene saturated aerogel floats on the water and can be removed after separation.

The absorption capacities of BSQ aerogels for various organic solvents and oils are shown in Figure 6b. The weight gains range from 1217 to 2889%, determined by the densities of the absorbed organic liquids because the pore volume of the aerogel is consistent. Though the weight gains are incomparable with some carbonaceous aerogels,[25,66,67] BSQ aerogels are competitive, since both the absorption capacity and the time to reach the absorption equilibrium should be considered for practical applications, such as dealing with oil spill accidents.

The robust mechanical property promises the BSQ aerogels facile desorption of the oil and good durability in cycling usage (Figure 7). The aerogels saturated by volatile organic liquids (Figure 7a–c) are robust enough to be vacuum-dried for use in the next cycle. In the case of pump oil (Figure 7d), which is difficult to volatilize, ethanol is used to expel the absorbed pump oil. During the cycling absorption–desorption processes, the aerogels maintain the adsorption capacity for at least five cycles.

The high separation speed, large volume uptake, and good reusability demonstrated the superhydrophobic BSQ aerogels as ideal candidates for separating and collecting organic pollutants or oil from oily wastewater.

3.5. Application in Sound Absorption. Aerogels have long been recognized as effective candidates for acoustic absorptions because the energy of sound waves could be significantly dissipated when passing through the interconnected pore structures.[68–70] The aerogels prepared from the different BSQ precursors show tunable sound absorption behaviors due to the distinct mechanical properties.

As shown in Figure 8, the BSQ aerogels show typical frequency-dependent sound absorption curves containing multiple resonant absorption peaks. The first resonant absorption peak of A1 with a maximum absorption coefficient of 84.8% appears at low frequency (1875 Hz), which is the most sensitive band to human ears.[71] The lightweight and high porous sound absorption material is easy to resonate with the

DOI: 10.1021/am5077765
ACS Appl. Mater. Interfaces 2015, 7, 2016–2024

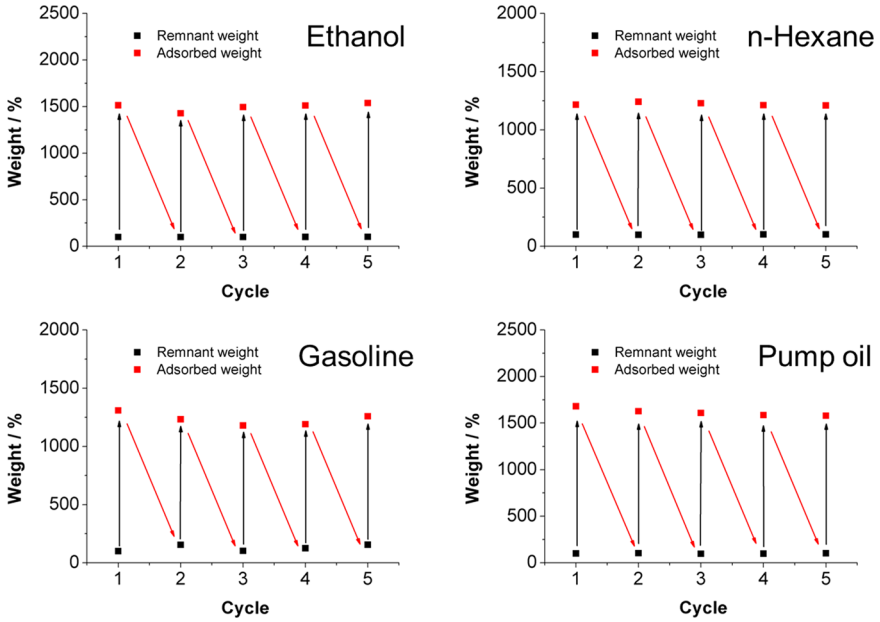

Figure 7. Absorption recyclability of the BSQ aerogels.

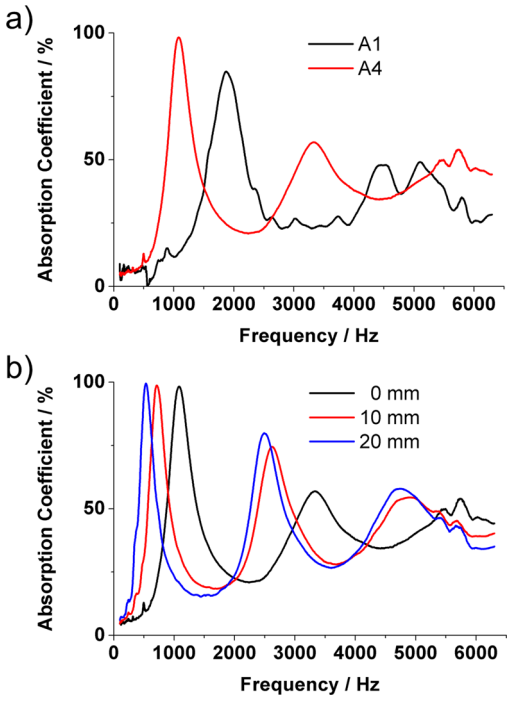

Figure 8. (a) Sound absorption coefficients of A1 and A4 with the back cavity of 0 mm. (b) Sound absorption coefficients of A4 with different back cavities.

low-frequency sound wave, and consequently gives a large absorption. When the frequency goes higher, harmonic frequency absorption peaks appear which are in agreement with previously reported silica aerogels.[72] As flexible materials are beneficial for low-frequency sound absorption,[73,74] the absorption coefficient shifting to an even lower frequency is observed in the case of A4. The maximum absorption coefficient at 1082 Hz even reaches as high as 98.3%. Over the whole frequency range, the average sound absorption of A4 has an increase of 6.8% compared with A1.

A typical Helmholtz resonator can be constructed with the aerogel and the back cavity.[75] The low-frequency sound wave forces the air within the aerogel pores to vibrate drastically in the resonator and sound energy dissipated seriously during the resonance. Therefore, along with the increasing back cavities, the maximum sound absorption frequency of A4 can shift to 535 Hz with a remarkable absorption coefficient of 99.5% with the back cavity of 20 mm (Figure 8b). Combining the low thermal conductivities (Table 1) and high and tunable sound absorption performances in an outstanding way, the BSQ aerogels promise potential application in the field of architecture.

4. CONCLUSIONS

BSQ precursors with various alkoxy groups have been synthesized using thiol-ene reactions. On the basis of the different hydrolyzing rates of the alkoxy groups, BSQ aerogels with tailorable morphology and mechanical performances can be obtained, while the densities are maintained at the same level. Noteworthy, although P2 and P3 contain the same proportion of methoxy and ethoxy groups, the resultant aerogels exhibit an obvious distinction because the alkoxy groups are connected in different ways. It is an adoptable method to tailor the performance of BSQ aerogels by using the distinct hydrolyzing rates of various alkoxy groups. Further, the highly porous, robust, and superhydrophobic BSQ aerogels have demonstrated their promising application in oil/water separation with good separation efficiency and recyclability, and shown the potential as ideal candidates for low-frequency sound absorption materials.

■ ASSOCIATED CONTENT

Supporting Information

Figures showing ^{1}H NMR spectra, FT-IR spectra, ^{13}C NMR spectra, TOF mass spectra, and pore size distribution. This material is available free of charge via the Internet at http://pubs.acs.org.

DOI: 10.1021/am5077765
ACS Appl. Mater. Interfaces 2015, 7, 2016−2024

AUTHOR INFORMATION

Corresponding Authors

*E-mail: zhaoning@iccas.ac.cn. Phone (Fax): +86 10 82619667. Postal address: Box 50, Zhongguancun North First Street 2, Beijing 100190, China.

*E-mail: jxu@iccas.ac.cn. Phone (Fax): +86 10 82619667. Postal address: Box 50, Zhongguancun North First Street 2, Beijing 100190, China.

Notes

The authors declare no competing financial interest.

ACKNOWLEDGMENTS

The authors thank MOST (2013CB933000) and NSFC (U1134105, 51373185, 21121001) for financial support.

REFERENCES

(1) Kistler, S. S. Coherent Expanded Aerogels and Jellies. *Nature* **1931**, *127*, 741−741.

(2) Husing, N.; Schubert, U. Aerogels Airy Materials: Chemistry, Structure, and Properties. *Angew. Chem., Int. Ed.* **1998**, *37*, 22−45.

(3) Dorcheh, A. S.; Abbasi, M. Silica Aerogel; Synthesis, Properties and Characterization. *J. Mater. Process. Technol.* **2008**, *199*, 10−26.

(4) Gesser, H. D.; Goswami, P. C. Aerogels and Related Porous Materials. *Chem. Rev.* **1989**, *89*, 765−788.

(5) Pierre, A. C.; Pajonk, G. M. Chemistry of Aerogels and Their Applications. *Chem. Rev.* **2002**, *102*, 4243−4265.

(6) Power, M.; Hosticka, B.; Black, E.; Daitch, C.; Norris, P. Aerogels as Biosensors: Viral Particle Detection by Bacteria Immobilized on Large Pore Aerogel. *J. Non-Cryst. Solids* **2001**, *285*, 303−308.

(7) Tsutsui, T.; Yahiro, M.; Yokogawa, H.; Kawano, K. Doubling Coupling-Out Efficiency in Organic Light-Emitting Devices Using a Thin Silica Aerogel Layer. *Adv. Mater.* **2001**, *13*, 1149−1152.

(8) Zu, G.; Shen, J.; Zou, L.; Wang, W.; Lian, Y.; Zhang, Z.; Du, A. Nanoengineering Super Heat-Resistant, Strong Alumina Aerogels. *Chem. Mater.* **2013**, *25*, 4757−4764.

(9) Cui, S.; Cheng, W.; Shen, X.; Fan, M.; Russell, A.; Wu, Z.; Yi, X. Mesoporous Amine-Modified SiO_2 Aerogel: A Potential CO_2 Sorbent. *Energy Environ. Sci.* **2011**, *4*, 2070−2074.

(10) Kettunen, M.; Silvennoinen, R. J.; Houbenov, N.; Nykänen, A.; Ruokolainen, J.; Sainio, J.; Pore, V.; Kemell, M.; Ankerfors, M.; Lindström, T.; Ritala, M.; Ras, R. H. A.; Ikkala, O. Photoswitchable Superabsorbency Based on Nanocellulose Aerogels. *Adv. Funct. Mater.* **2011**, *21*, 510−517.

(11) Qiu, B.; Xing, M.; Zhang, J. Mesoporous TiO_2 Nanocrystals Grown in Situ on Graphene Aerogels for High Photocatalysis and Lithium-Ion Batteries. *J. Am. Chem. Soc.* **2014**, *136*, 5852−5855.

(12) Jung, S. M.; Jung, H. Y.; Fang, W.; Dresselhaus, M. S.; Kong, J. A Facile Methodology for the Production of in Situ Inorganic Nanowire Hydrogels/Aerogels. *Nano Lett.* **2014**, *14*, 1810−1817.

(13) Meador, M. A. B.; Wright, S.; Sandberg, A.; Nguyen, B. N.; Van Keuls, F. W.; Mueller, C. H.; Rodríguez-Solís, R.; Miranda, F. A. Low Dielectric Polyimide Aerogels as Substrates for Lightweight Patch Antennas. *ACS Appl. Mater. Interfaces* **2012**, *4*, 6346−6353.

(14) Randall, J. P.; Meador, M. A. B.; Jana, S. C. Tailoring Mechanical Properties of Aerogels for Aerospace Applications. *ACS Appl. Mater. Interfaces* **2011**, *3*, 613−626.

(15) Fellinger, T.-P.; White, R. J.; Titirici, M.-M.; Antonietti, M. Borax-Mediated Formation of Carbon Aerogels from Glucose. *Adv. Funct. Mater.* **2012**, *22*, 3254−3260.

(16) Nardecchia, S.; Carriazo, D.; Ferrer, M. L.; Gutierrez, M. C.; del Monte, F. Three Dimensional Macroporous Architectures and Aerogels Built of Carbon Nanotubes and/or Graphene: Synthesis and Applications. *Chem. Soc. Rev.* **2013**, *42*, 794−830.

(17) Peng, Q.; Li, Y.; He, X.; Gui, X.; Shang, Y.; Wang, C.; Wang, C.; Zhao, W.; Du, S.; Shi, E.; Li, P.; Wu, D.; Cao, A. Graphene Nanoribbon Aerogels Unzipped from Carbon Nanotube Sponges. *Adv. Mater.* **2014**, *26*, 3241−3247.

(18) Antonietti, M.; Fechler, N.; Fellinger, T.-P. Carbon Aerogels and Monoliths: Control of Porosity and Nanoarchitecture via Sol-Gel Routes. *Chem. Mater.* **2013**, *26*, 196−210.

(19) Qiu, L.; Liu, J. Z.; Chang, S. L.; Wu, Y.; Li, D. Biomimetic Superelastic Graphene-Based Cellular Monoliths. *Nat. Commun.* **2012**, *3*, 1241.

(20) Li, C.; Shi, G. Functional Gels Based on Chemically Modified Graphenes. *Adv. Mater.* **2014**, *26*, 3992−4012.

(21) Yang, Z.-Y.; Jin, L.-J.; Lu, G.-Q.; Xiao, Q.-Q.; Zhang, Y.-X.; Jing, L.; Zhang, X.-X.; Yan, Y.-M.; Sun, K.-N. Sponge-Templated Preparation of High Surface Area Graphene with Ultrahigh Capacitive Deionization Performance. *Adv. Funct. Mater.* **2014**, *24*, 3917−3925.

(22) Wu, X.-L.; Wen, T.; Guo, H.-L.; Yang, S.; Wang, X.; Xu, A.-W. Biomass-Derived Sponge-Like Carbonaceous Hydrogels and Aerogels for Supercapacitors. *ACS Nano* **2013**, *7*, 3589−3597.

(23) Wu, Z.-S.; Yang, S.; Sun, Y.; Parvez, K.; Feng, X.; Müllen, K. 3D Nitrogen-Doped Graphene Aerogel-Supported Fe_3O_4 Nanoparticles as Efficient Electrocatalysts for the Oxygen Reduction Reaction. *J. Am. Chem. Soc.* **2012**, *134*, 9082−9085.

(24) Bi, H.; Huang, X.; Wu, X.; Cao, X.; Tan, C.; Yin, Z.; Lu, X.; Sun, L.; Zhang, H. Carbon Microbelt Aerogel Prepared by Waste Paper: An Efficient and Recyclable Sorbent for Oils and Organic Solvents. *Small* **2014**, *10*, 3544−3550.

(25) Sun, H.; Xu, Z.; Gao, C. Multifunctional, Ultra-Flyweight, Synergistically Assembled Carbon Aerogels. *Adv. Mater.* **2013**, *25*, 2554−2560.

(26) Wang, X.; Jana, S. C. Synergistic Hybrid Organic-Inorganic Aerogels. *ACS Appl. Mater. Interfaces* **2013**, *5*, 6423−6429.

(27) Randall, J. P.; Meador, M. A. B.; Jana, S. C. Polymer Reinforced Silica Aerogels: Effects of Dimethyldiethoxysilane and Bis-(Trimethoxysilylpropyl)Amine as Silane Precursors. *J. Mater. Chem. A* **2013**, *1*, 6642−6652.

(28) Cai, J.; Liu, S.; Feng, J.; Kimura, S.; Wada, M.; Kuga, S.; Zhang, L. Cellulose-Silica Nanocomposite Aerogels by in Situ Formation of Silica in Cellulose Gel. *Angew. Chem., Int. Ed.* **2012**, *51*, 2076−2079.

(29) Kobayashi, Y.; Saito, T.; Isogai, A. Aerogels With 3D Ordered Nanofiber Skeletons of Liquid-Crystalline Nanocellulose Derivatives as Tough and Transparent Insulators. *Angew. Chem., Int. Ed.* **2014**, *53*, 10394−10397.

(30) Fidalgo, A.; Farinha, J. P. S.; Martinho, J. M. G.; Rosa, M. E.; Ilharco, L. M. Hybrid Silica/Polymer Aerogels Dried at Ambient Pressure. *Chem. Mater.* **2007**, *19*, 2603−2609.

(31) Dutoit, D. C. M.; Schneider, M.; Fabrizioli, P.; Baiker, A. Vanadia-Silica Low-Temperature Aerogels: Influence of Aging and Vanadia Loading on Structural and Chemical Properties. *Chem. Mater.* **1996**, *8*, 734−743.

(32) Loy, D. A.; Shea, K. J. Bridged Polysilsesquioxanes. Highly Porous Hybrid Organic-Inorganic Materials. *Chem. Rev.* **1995**, *95*, 1431−1442.

(33) Shea, K. J.; Loy, D. A. Bridged Polysilsesquioxanes. Molecular-Engineered Hybrid Organic-Inorganic Materials. *Chem. Mater.* **2001**, *13*, 3306−3319.

(34) Eckstorff, F.; Zhu, Y.; Maurer, R.; Müller, T. E.; Scholz, S.; Lercher, J. A. Materials with Tunable Low-k Dielectric Constant Derived from Functionalized Octahedral Silsesquioxanes and Spherosilicates. *Polymer* **2011**, *52*, 2492−2498.

(35) Hu, L.-C.; Shea, K. J. Organo-Silica Hybrid Functional Nanomaterials: How Do Organic Bridging Groups and Silsesquioxane Moieties Work Hand-in-Hand? *Chem. Soc. Rev.* **2011**, *40*, 688−695.

(36) Kim, J. H.; Fang, B.; Song, M. Y.; Yu, J.-S. Topological Transformation of Thioether-Bridged Organosilicas into Nanostructured Functional Materials. *Chem. Mater.* **2012**, *24*, 2256−2264.

(37) Liang, X.; Li, X.; Yue, X.; Dai, Z. Conjugation of Porphyrin to Nanohybrid Cerasomes for Photodynamic Diagnosis and Therapy of Cancer. *Angew. Chem., Int. Ed.* **2011**, *50*, 11622−11627.

(38) Boday, D. J.; Stover, R. J.; Muriithi, B.; Loy, D. A. Strong, Low Density, Hexylene- and Phenylene-Bridged Polysilsesquioxane Aerogel-Polycyanoacrylate Composites. *J. Mater. Sci.* **2011**, *46*, 6371−6377.

DOI: 10.1021/am5077765
ACS Appl. Mater. Interfaces 2015, 7, 2016−2024

(39) Wang, Z.; Dai, Z.; Wu, J.; Zhao, N.; Xu, J. Vacuum-Dried Robust Bridged Silsesquioxane Aerogels. *Adv. Mater.* **2013**, *25*, 4494−4497.
(40) Guo, H. Q.; Nguyen, B. N.; McCorkle, L. S.; Shonkwiler, B.; Meador, M. A. B. Elastic Low Density Aerogels Derived from Bis[3-(Triethoxysilyl)Propyl]Disulfide, Tetramethylorthosilicate and Vinyltrimethoxysilane via a Two-Step Process. *J. Mater. Chem.* **2009**, *19*, 9054−9062.
(41) Loy, D. A.; Jamison, G. M.; Baugher, B. M.; Russick, E. M.; Assink, R. A.; Prabakar, S.; Shea, K. J. Alkylene-Bridged Polysilsesquioxane Aerogels: Highly Porous Hybrid Organic-Inorganic Materials. *J. Non-Cryst. Solids* **1995**, *186*, 44−53.
(42) Kuroda, K.; Shimojima, A.; Kawahara, K.; Wakabayashi, R.; Tamura, Y.; Asakura, Y.; Kitahara, M. Utilization of Alkoxysilyl Groups for the Creation of Structurally Controlled Siloxane-Based Nanomaterials. *Chem. Mater.* **2014**, *26*, 211−220.
(43) Yamada, H.; Urata, C.; Aoyama, Y.; Osada, S.; Yamauchi, Y.; Kuroda, K. Preparation of Colloidal Mesoporous Silica Nanoparticles with Different Diameters and Their Unique Degradation Behavior in Static Aqueous Systems. *Chem. Mater.* **2012**, *24*, 1462−1471.
(44) Yano, K.; Fukushima, Y. Particle Size Control of Mono-Dispersed Super-Microporous Silica Spheres. *J. Mater. Chem.* **2003**, *13*, 2577−2581.
(45) Sarawade, P.; Kim, J.; Kim, H.; Kim, H. High Specific Surface Area TEOS-Based Aerogels with Large Pore Volume Prepared at an Ambient Pressure. *Appl. Surf. Sci.* **2007**, *254*, 574−579.
(46) Tucker-Schwartz, A. K.; Farrell, R. A.; Garrell, R. L. Thiol-Ene Click Reaction as a General Route to Functional Trialkoxysilanes for Surface Coating Applications. *J. Am. Chem. Soc.* **2011**, *133*, 11026−11029.
(47) Shih, H.; Lin, C.-C. Cross-Linking and Degradation of Step-Growth Hydrogels Formed By Thiol-Ene Photoclick Chemistry. *Biomacromolecules* **2012**, *13*, 2003−2012.
(48) Lin, H.; Wan, X.; Jiang, X.; Wang, Q.; Yin, J. A Nanoimprint Lithography Hybrid Photoresist Based on the Thiol-Ene System. *Adv. Funct. Mater.* **2011**, *21*, 2960−2967.
(49) Hoogenboom, R. Thiol-Yne Chemistry: A Powerful Tool for Creating Highly Functional Materials. *Angew. Chem., Int. Ed.* **2010**, *49*, 3415−3417.
(50) Lowe, A. B. Thiol-Ene "Click" Reactions and Recent Applications in Polymer and Materials Synthesis: A First Update. *Polym. Chem.* **2014**, *5*, 4820−4870.
(51) Hoyle, C. E.; Bowman, C. N. Thiol-Ene Click Chemistry. *Angew. Chem., Int. Ed.* **2010**, *49*, 1540−1573.
(52) Noisser, T.; Reichenauer, G.; Husing, N. In Situ Modification of the Silica Backbone Leading to Highly Porous Monolithic Hybrid Organic-Inorganic Materials via Ambient Pressure Drying. *ACS Appl. Mater. Interfaces* **2014**, *6*, 1025−1029.
(53) Rao, A. V.; Nilsen, E.; Einarsrud, M. A. Effect of Precursors, Methylation Agents and Solvents on the Physicochemical Properties of Silica Aerogels Prepared by Atmospheric Pressure Drying Method. *J. Non-Cryst. Solids* **2001**, *296*, 165−171.
(54) Smith, D. M.; Scherer, G. W.; Anderson, J. M. Shrinkage during Drying of Silica Gel. *J. Non-Cryst. Solids* **1995**, *188*, 191−206.
(55) Loy, D. A.; Russick, E. M.; Yamanaka, S. A.; Baugher, B. M.; Shea, K. J. Direct Formation of Aerogels by Sol-Gel Polymerizations of Alkoxysilanes in Supercritical Carbon Dioxide. *Chem. Mater.* **1997**, *9*, 2264−2268.
(56) Loy, D. A.; Baugher, B. M.; Baugher, C. R.; Schneider, D. A.; Rahimian, K. Substituent Effects on the Sol-Gel Chemistry of Organotrialkoxysilanes. *Chem. Mater.* **2000**, *12*, 3624−3632.
(57) Xiang, S.; Li, L.; Zhang, J.; Tan, X.; Cui, H.; Shi, J.; Hu, Y.; Chen, L.; Su, C.-Y.; James, S. L. Porous Organic-Inorganic Hybrid Aerogels Based on Cr^{3+}/Fe^{3+} and Rigid Bridging Carboxylates. *J. Mater. Chem.* **2012**, *22*, 1862−1867.
(58) Kruk, M.; Jaroniec, M. Gas Adsorption Characterization of Ordered Organic-Inorganic Nanocomposite Materials. *Chem. Mater.* **2001**, *13*, 3169−3183.
(59) Lu, X.; Arduinischuster, M. C.; Kuhn, J.; Nilsson, O.; Fricke, J.; Pekala, R. W. Thermal-Conductivity of Monolithic Organic Aerogels. *Science* **1992**, *255*, 971−972.
(60) Moner-Girona, M.; Roig, A.; Molins, E.; Martinez, E.; Esteve, J. Micromechanical Properties of Silica Aerogels. *Appl. Phys. Lett.* **1999**, *75*, 653−655.
(61) Tillotson, T. M.; Hrubesh, L. W. Transparent Ultralow-Density Silica Aerogels Prepared by a 2-Step Sol-Gel Process. *J. Non-Cryst. Solids* **1992**, *145*, 44−50.
(62) Feng, L.; Li, S.; Li, Y.; Li, H.; Zhang, L.; Zhai, J.; Song, Y.; Liu, B.; Jiang, L.; Zhu, D. Super-Hydrophobic Surfaces: From Natural to Artificial. *Adv. Mater.* **2002**, *14*, 1857−1860.
(63) Wang, X.; Jana, S. C. Tailoring of Morphology and Surface Properties of Syndiotactic Polystyrene Aerogels. *Langmuir* **2013**, *29*, 5589−5598.
(64) Duan, Y.; Jana, S. C.; Reinsel, A. M.; Lama, B.; Espe, M. P. Surface Modification and Reinforcement of Silica Aerogels Using Polyhedral Oligomeric Silsesquioxanes. *Langmuir* **2012**, *28*, 15362−15371.
(65) Wang, X.; Jana, S. C. Synergistic Hybrid Organic-Inorganic Aerogels. *ACS Appl. Mater. Interfaces* **2013**, *5*, 6423−6429.
(66) Wu, Z.-Y.; Li, C.; Liang, H.-W.; Chen, J.-F.; Yu, S.-H. Ultralight, Flexible, and Fire-Resistant Carbon Nanofiber Aerogels from Bacterial Cellulose. *Angew. Chem., Int. Ed.* **2013**, *52*, 2925−2929.
(67) Bi, H.; Yin, Z.; Cao, X.; Xie, X.; Tan, C.; Huang, X.; Chen, B.; Chen, F.; Yang, Q.; Bu, X.; Lu, X.; Sun, L.; Zhang, H. Carbon Fiber Aerogel Made from Raw Cotton: A Novel, Efficient and Recyclable Sorbent for Oils and Organic Solvents. *Adv. Mater.* **2013**, *25*, 5916−5921.
(68) Bheekhun, N.; Abu Talib, A. R.; Hassan, M. R. Aerogels in Aerospace: An Overview. *Adv. Mater. Sci. Eng.* **2013**, 406065.
(69) Baetens, R.; Jelle, B. P.; Gustavsen, A. Aerogel Insulation for Building Applications: A State-of-the-Art Review. *Energy Build.* **2011**, *43*, 761−769.
(70) Nakajima, H. Fabrication, Properties and Application of Porous Metals with Directional Pores. *Prog. Mater. Sci.* **2007**, *52*, 1091−1173.
(71) Schmidt, M.; Schwertfeger, F. Applications for Silica Aerogel Products. *J. Non-Cryst. Solids* **1998**, *225*, 364−368.
(72) Wang, J.; Shen, J.; Ni, X.; Wang, B.; Wang, X.; Li, J. Acoustic Properties of Nanoporous Silica Aerogel. *Rare Met. Mater. Eng.* **2010**, *39*, 14−17.
(73) Wassilieff, C. Sound Absorption of Wood-Based Materials. *Appl. Acoust.* **1996**, *48*, 339−356.
(74) Fouladi, M. H.; Ayub, M.; Nor, M. J. M. Analysis of Coir Fiber Acoustical Characteristics. *Appl. Acoust.* **2011**, *72*, 35−42.
(75) Zhang, S.; Yin, L.; Fang, N. Focusing Ultrasound with an Acoustic Metamaterial Network. *Phys. Rev. Lett.* **2009**, *102*, 194301.

DOI: 10.1021/am5077765
ACS Appl. Mater. Interfaces 2015, 7, 2016−2024